Simulating the microfluidic solvent extraction of perrhenate

Investigating the influence of pH and leakage

by

Miranda van Duijn

to obtain the degree of Bachelor of Science
at the Delft University of Technology,
to be defended publicly on Tuesday January 23, 2018 at 10:00 AM.

Student number:	4355776	
Project duration:	September, 2017 – January 23, 2018	
Thesis committee:	Ir. Z. Liu,	TU Delft, supervisor
	Dr. ir. M. Rohde,	TU Delft
	Prof. dr. ir. J.L. Kloosterman	TU Delft

TU Delft

Abstract

Several of the researches conducted at the Reactor Institute Delft (RID) concern the extraction process of perrhenate, ReO_4^-. From the perrhenate, rhenium-188 (Re-188) is obtained. Re-188 is medically useful as a high energy β emitter. It can be used as an imaging agent, for in situ tumor treatment and biodistribution. Re-188 is produced via commercially available $^{188}W/^{188}Re$ radionuclide generators, which have proved their usefulness as a conventional product. Via the production with this generator, the ReO_4^- resides in an aqueous solution together with other compounds such as tungsten-188 (W-188). To medically use the ReO_4^-, it needs to be of a certain degree of radionuclidic purity, the proportion of the total radioactivity that is present as a specific radionuclide. [1]

A relatively new method to extract the ReO_4^- from the aqueous solution into a liquid organic phase might be microfluidic solvent extraction. This principle is based on the laminar coflowing of two liquid immiscible phases between which an interface develops. The ReO_4^- is then transferred through the interface, thus leading to an extraction.

Microfluidic solvent extraction offers several inherent advantages, such as the high surface-to-volume ratio and short diffusion distances. Also, with microfluidics, extraction processes can be eventually engineered onto a lab-on-a-chip, which offers easy operation and reduction of radioactive shielding.

In a previous study done by Dalmázio and Oehlke [5], an experimental set-up with a microfluidic channel of 12[cm] length and two inlets and outlets in a Y configuration was used to establish a stable interface for aqueous solutions and methyl-ethyl-ketone(MEK) as organic phase. For several HCl concentrations in the aqueous phase, the extraction efficiency was measured via gamma counting. The highest extraction efficiency occurred for 1 [M] HCl concentrations and amounts 52.00%. In this experiment, leakage from the organic phase to the aqueous phase was observed.

This research focuses on the influence of several parameters on the extraction efficiency. The concentration profiles of the ReO_4^- in both phases depend on, among others, the diffusion coefficent and distribution ratio. The distribution ratio is in turn dependent on the pH and thus the equilibrium reaction of the ReO_4^- to perrhenic acid ($HReO_4$) in the aqueous phase. A model in COMSOL was made, using several assumptions which were based on experimental results of Dalmázio and Oehlke and theory. A parametric sweep for the diffusion coefficent, distribution ratio, mass transfer coefficient and flow rate was made and analysed. Also, the obtained results were compared for extraction with and without leakage for the optimal parameter values.

The optimal parameter combination is a high diffusion coefficient in both the organic and aqueous phase, high mass transfer coefficient and low flow rate. The maximum extraction efficiency amounts 62.16% without leakage accounted for and 27.20% with the leakage accounted for. For this optimum, the distribution ratio $M = 106$ and diffusion coefficient $D = 1 \cdot 10^{-9} m^2/s$ in the aqueous and organic phase have been estimated on previous studies. The leakage has been evaluated for several situations and on average, the extraction efficiency is 2.5 times higher when there is no leakage. When the distribtion ratio is increased even more to $M = 1000$, the extraction effiency without the leakage accounted for only increases to 62.66%. This hints to asymptotic behaviour of the extraction efficiency depending on the distribution ratio. The results from the model were compared to the experimental results by Dalmázio and Oehlke, and a big deviation has been observed. This can be assigned to the unknown or incorrectly estimated parameters. Lastly, it is concluded that not the ReO_4^-, but $HReO_4$ diffuses through the interface.

Miranda van Duijn
Delft, January 2018

Contents

1 Introduction

Research which is being done at the reactor concerning radionuclides At the Reactor Institute of Delft (RID), research is being done on the extraction efficiencies of radioactive isotopes in a solution, using microfluidic solvent extraction. Microfluidic solvent extraction is based on the laminar, co-parallel flow of two immiscible phases in a microfluidic channel on a chip. The compound is extracted through the established interface. This paper will focus on the extraction of ReO_4^-, from an aqueous solution using methyl-ethyl-ketone (MEK) as solvent. ReO_4^- is one of the oxoanions in which Re-188 is present, a high energy β-emitting radioisotope. [10]

Advantages microfluidics and microfluidic chips Microfluidics is a relatively new field of study and offers several advantages compared to conventional fluidics in multiple applications. Microfluidic devices can be used for microchemical synthesis, liquid-liquid extraction of radionuclides, controlled mixing of chemical compounds and small molecule analysis [5]. In microfluidics, laminar flow can be used and there is automatically a high surface-to-volume ratio and short diffusion distance. Resulting in less waste production and smaller volumes needed thus also a cost reduction. When microfluidic extraction is done in several subsequent cascades, even smaller volumes are needed. [7]

Uses of perrhenate and similarities to other medical useful radio-isotopes. Re-188 has proved its usefulness in several medical applications; imaging, in situ treatment of cancerous tissue and radiotherapy, due to its physical properties. Re-188 is produced via a $^{188}W/^{188}Re$ radionuclide generator. In this generator, the radionuclide is available as the oxoanion ReO_4^-. This radionuclide generator is widely used, for example in hospitals because it has a long shelf-life and thus is costly beneficial. Via this production method, the ReO_4^- resides in the aqueous solution together with, among other compounds, W-188, from which it needs to be separated. [10] Furthermore, Re-188 is similar to Tc-99m because of the similar electronic configuration and stereochemistry. Even though rhenium resides in a different row in the periodic system, the ionic radii of the elements are alike due to a phenomenon called the lanthanide contraction. Thus, research about Re-188 extraction is also applicable to Tc-99m and vice versa. This is very useful, as Tc-99m has a short half-life of 6 hours and is one of the most widely used radioactive isotopes for medical imaging. [13]

Results of paper of Dalmázio and Oehlke In a study done by Dalmázio and Oehlke [5] the liquid-liquid extraction of ReO_4^- was investigated. In a Y-shaped microfluidic channel, via one inlet an aqueous solution containing ammonium perrhenate (NH_4ReO_4) was pushed through the channel. Through the second inlet, an organic liquid phase was pushed and a stable interface was realised by testing several flow conditions. Furthermore, the influence of adding hydrogen chloride (HCl) to the aqueous solution was examined. The extraction efficiency increased when the contact time was increased. Furthermore, it can be concluded that the extraction efficiency increased as the concentration of HCl increased in the aqueous solution. For a 0.1 [g/mL] aqueous ReO_4^- solution with 1 [mol/L] HCl added and a contact time of 1.1 [s], the extraction efficiency was found to be 52.00%.

Investigating the mechanism of extraction by simulating In this research, the liquid-liquid extraction of ReO_4^- is investigated, by constructing a model in COMSOL based on theory and empirical estimations. The extraction takes place only via diffusion and is hence called inactive, as opposed to active extraction which also includes a chemical extraction reaction. In the model, a laminar, two-phase flow is simulated and evaluated using the finite element method (FEM). The microfluidics are governed by the incompressible Navier-Stokes equations and Fick's laws. These equations depend on diffusion coefficients, mass transfer coefficients and distribution ratios. For these coefficients, a parametric sweep was made to try and match the simulated results to the experimental results of Dalmázio and Oehlke. This provides insight in the influence of these parameters on the extraction efficiency. The model has been made, with and without accounting for the leakage, to also give insight in the influence of the leakage on the extraction efficiency.

2

Theory

2.1. Microfluidics

Microfluidics is the field which describes the manipulation of fluids that are to be found in geometrically small spaces. Typically, the scale that is associated with microfluidics is below the millimetre scale. In this project it was applicable because of the small width of the channel, even though the channel is 12cm in length.

The behaviour of fluids at microscopic level can be described by the Navier-Stokes equations and the so-called continuity equation. These are derived from the principles of conservation of momentum and mass respectively. When dealing with fluids, continuum materials, characteristics such as mass and force need to be described by their continuum forms; density ρ and force density $\mathbf{f}$. [4]

2.1.1. Continuity equation

The continuity equation is derived from the mass conservation principle. When an arbitrarily shaped control volume $d\Omega$ is considered, then the total mass contained within that control volume at time t is

$$M(\Omega, t) = \int \rho d\Omega \tag{2.1}$$

The rate of change of mass within the control volume equals what flows in and out through the boundaries Γ plus what is created or consumed by sources and sinks inside the control volume

$$\frac{d}{dt}\int_\Omega \rho d\Omega = -\int_\Gamma \rho \mathbf{u}\cdot\mathbf{n} d\Gamma - \int_\Omega s d\Omega \tag{2.2}$$

where $\mathbf{u}$ flow velocity of the fluid, $\mathbf{n}$ is the outward-pointing unit-normal vector and $\mathbf{s}$ embodies the sinks and sources. Setting the sinks and sources within Ω to zero, and applying Gauss's theorem to the surface integral over Γ leads to

$$\frac{d}{dt}\int_\Omega d\Omega = -\int_\Omega \nabla\cdot(\rho\mathbf{u}) d\Omega - \int_\Omega \mathbf{s} d\Omega \tag{2.3}$$

Then, with Reynolds transport theorem applied to the left side of the equation

$$\int_\Omega \frac{\partial \rho}{\partial t} d\Omega = -\int_\Omega \nabla\cdot(\rho\mathbf{u}) d\Omega - \int_\Omega s d\Omega \tag{2.4}$$

and combining all of the integrals

$$\int_\Omega \left(\frac{\partial \rho}{\partial t} + \nabla\cdot(\rho\mathbf{u}) + s\right) d\Omega = 0 \tag{2.5}$$

As the integral is zero for any control volume, the integrand itself must be zero, yielding the continuity equation

$$\frac{\partial \rho}{\partial t} + \nabla\cdot\left(\rho\mathbf{u}\right) = 0 \tag{2.6}$$

with the mass flux appearing in the continuity equation as

$$\phi_m(\mathbf{r}, t) = \rho(\mathbf{r}, t)\cdot\mathbf{u}(\mathbf{r}, t) \tag{2.7}$$

2.1.2. The Navier-Stokes equations

The Navier-Stokes equations are the continuum counterpart of Newton's second law. The equations are derived from the principle of conservation of momentum. The rate of change of momentum within the control volume Ω equals what flows in and out through the boundaries Γ plus the production or consumption within that control volume. The material derivative, as defined in formula 2.8, is used to describe the rate of change of momentum in a macroscopic velocity field of a material element. This macroscopic velocity field is space-and-time-dependent.

$$\frac{D}{Dt} \equiv \frac{\partial}{\partial t} + \mathbf{u} \cdot \nabla \tag{2.8}$$

With the momentum density $\rho\mathbf{u}$, this yields

$$\frac{\partial}{\partial t}(\rho\mathbf{u}) + \nabla \cdot (\rho\mathbf{u}\mathbf{u}) \tag{2.9}$$

by doing some vector calculus, we get [15]

$$\rho\left(\frac{\partial \mathbf{u}}{\partial t} + \mathbf{u} \cdot \nabla\mathbf{u}\right) = \mathbf{s} \tag{2.10}$$

Where $\mathbf{s}$, the rate of change in momentum, equals the sum of forces acting on the control volume, which follows from Newton's second law

$$\mathbf{s} = \mathbf{f}_{pressure} + \mathbf{f}_{viscous} + \mathbf{f}_{body} \tag{2.11}$$

Where the body force densities are due to gravitational forces, electrical forces and magnetic forces within the fluid. The pressure force density is given by

$$\mathbf{f}_{pressure} = \frac{\mathbf{F}_{pressure}}{V} = -\nabla P \tag{2.12}$$

The viscous force density is given by

$$\mathbf{f}_{viscous} = \frac{\mathbf{F}_{viscous}}{V} = \mu\nabla^2\mathbf{u} \tag{2.13}$$

with μ is the dynamic viscosity of the liquid. This expression holds for Newtonian fluids; the stress is linearly proportional to the strain. Combining the equations 2.11, 2.12 and 2.13, we arrive at the Navier-Stokes equations

$$\rho\left(\frac{\partial \mathbf{u}}{\partial t} + (\mathbf{u} \cdot \nabla\mathbf{u})\right) = -\nabla P + \mu\nabla^2\mathbf{u} \tag{2.14}$$

Navier-Stokes for an incompressible fluid For an incompressible fluid, [16]

$$\frac{\partial \rho}{\partial t} = 0 \tag{2.15}$$

ρ is constant over time and space thus the continuity equation reduces to

$$\nabla \cdot \mathbf{u} = 0 \tag{2.16}$$

and using this, and for laminar, parallel flow without external forces, the Navier-Stokes equation reduces to

$$\rho\left(\frac{\partial \mathbf{u}}{\partial t} + (\mathbf{u} \cdot \nabla)\right) = \mathbf{f}_{pressure} + \mathbf{f}_{viscous} + \mathbf{f}_{body} \tag{2.17}$$

2.1.3. Laminar two phase flow

Furthermore, at really small scales, multiple physical phenomena happen to coincide, complicating the description of the physics. Using dimensionless numbers is a common solution.

Reynolds number The flow type of the concerned fluid is important as it affects the mass transfer in the fluid system. Flow type ranges from turbulent to laminar. Laminar flow refers to a flow without lateral mixing, meaning that the fluid flows in neat, parallel layers. The laminarity of the flow can be characterised by the Reynolds number, Re [8]

$$Re = \frac{\rho < u > D_L}{\mu} \tag{2.18}$$

With $< u >$ is the average velocity of the flow and D_L the characteristic length of the flow, also known as the hydraulic diameter. The Reynolds number is therefore the ratio of the inertial force to the viscous force. This is an indication of how fast the fluid is moving relative to how viscous it is, giving the degree of laminarity. Because the characteristic lengths in microfluidics are adequately small, laminar flow regimes are realised.

Peclet number Laminar flow has high momentum diffusion and low momentum convection. Thus, the momentum transport in the y-direction is mainly due to diffusion when laminar flow regimes are considered. The Peclet number, Pe, indicates the ratio between diffusion and convection. The Peclet number is given as

$$Pe = \frac{< u > L}{D} \tag{2.19}$$

with L the characteristic length of the system perpendicular to the flow and D the diffusion coefficient.

Velocity profile Poiseuille flow The velocity profile of the two phase flow plays a role in the extraction, as it influences the contact time between the two phases and also the speed in which the molecules are convected. The flow in the experiment is Poiseuille flow, as the fluid can be considered to be in between two stationary infinite plate, under a constant pressure gradient in the x-direction. [6]

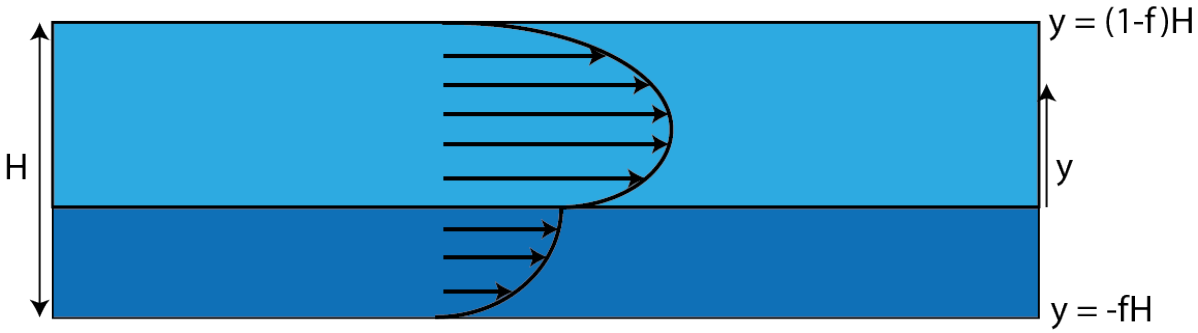

Figure 2.1: Schematic presentation of the flow profile of two-phase Poiseuille flow in a channel.

In figure 2.1, a two-phase flow between two plates is considered, the lower fluid taking up the fraction f of the volume. The stress profiles are

$$\tau_{org} = \frac{\nabla p}{L} y + C_1 \tag{2.20}$$

$$\tau_{aq} = \frac{\nabla p}{L} y + C_2 \tag{2.21}$$

Because the shear stress at the interface, y = 0, is continuous, $C_1 = C_2$ For Newtonian fluids we can write Newton's viscosity law

$$\tau = -\mu \frac{dv}{dy} \tag{2.22}$$

Inserting equation 2.22 in equations 2.20 and 2.21 results in

$$-\mu_{org} \frac{dv_{org}}{dy} = \frac{\nabla p}{L} y + C_1 \tag{2.23}$$

$$-\mu_{aq} \frac{dv_{aq}}{dy} = \frac{\nabla p}{L} y + C_1 \tag{2.24}$$

Integrating these equations gives parabolic flow profiles

$$v_{org,x} = -\frac{\nabla p}{2\mu_{org}L}y^2 - \frac{C_1}{\mu_{org}}y + C_2 \tag{2.25}$$

$$v_{aq,x} = -\frac{\nabla p}{2\mu_{aq}L}y^2 - \frac{C_1}{\mu_{aq}}y + C_2 \tag{2.26}$$

The constants can be solved by applying the no-slip boundary conditions at the wall

$$v_{org}(-fH) = v_{aq}[(1-f)H] = 0 \tag{2.27}$$

This results in

$$C_1 = \frac{\nabla pH}{2L}\frac{\mu_{aq}f^2 - \mu_{org}(1-f)^2}{f\mu_{aq} + (1-f)\mu_{org}} \tag{2.28}$$

$$C_2 = \frac{\nabla pH^2}{2L}\frac{f(1-f)}{f\mu_{aq} + (1-f)\mu_{org}} \tag{2.29}$$

2.1.4. Interface

Between the two phases, a stable interface may develop. In microfluidics, the surface phenomena's role becomes comparable to the role of potential energy forces. Attempting to establish a stable interface is called surface control. Theory behind the shape and location of the interface is needed to understand what is happening there. In this section, the interface stability between two phases flowing laminarly in a rectangular microchannel is discussed. Next, when the stability is assumed, the interface shape will be elaborated on.

Stable interface Previous study done by A. Blok [blok] [3], it has been derived that the interface in a rectangular microchannel can only stabilise when the microchannel has a maximum length. This length is given by

$$L = \frac{2dw^2\sigma_{12}sin(\theta - 90)}{\alpha\dot{V}_{aq}\mu_{aq}\left[1 - \frac{\mu_{org}}{\mu_{aq}}^{0.24}\right]} \tag{2.30}$$

with d the height of the channel, w half the width of the channel, σ_{12} the surface tension between phase 1 and 2 and $\dot{V}$ the volumetric flow rate of the aqueous phase. α is a constant given by

$$\alpha = \frac{22}{7}\frac{2w+d}{wd} - \frac{65}{3} \tag{2.31}$$

This equation holds for imiscible fluids. When two fluids are miscible, they might mix and a diffusion interface can develop. Studies have shown that the interface slowly smears but the smearing is significantly small when compared to the motion of the fluids. [14] An analogue to the Rayleigh number is introduced which is the ratio between diffusive and convective time scales, thus giving a sense of the smearing of the interface.

$$Ra_s = \frac{g\nabla\rho L^3}{\mu D} \tag{2.32}$$

Interface shape In two-phase liquid-liquid microfludic systems, surface phenomena may dominate. This will result in a curved interface shape, which in turn will affect the flow characteristics. The interface curvature can be deduced from energy considerations. Whether the interface takes a concave or convex surface, depends on the relative wettability properties of the two fluids with the walls. [12]

The stable interface configuration corresponds with minimal energy in the system and the reference point is a planar interface. The energy difference over unit length of a horizontal channel of length L is given by

$$\frac{\nabla E}{L} = \frac{1}{L}\nabla(E_p + E_s) \tag{2.33}$$

Where E_p is the energy associated with the potential energy and E_s the energy associated with surface energy.

The change in surface energy when the contact area between the two phases and the walls is varied is given by

$$\nabla E_s = (\nabla E_s)_{1w} + (\nabla E_s)_{2w} + (\nabla E_s)_{12} = \sigma_{1w}\nabla S_{1w} + \sigma_{2w}\nabla S_{2w} + \sigma_{12}\nabla S_{12} \tag{2.34}$$

Where the subscripts $\sigma_{1w}, \sigma_{2w}, \sigma_{12}$ denote the surface tensions between phase 1 and the wall, between phase 2 and the wall and between phase 1 and 2. ∇S denotes the change in surface area when the interface becomes more curved.
The change in contact area between the phases and the walls are

$$\frac{\nabla S_{2w}}{L} = 2R(\phi_0 - \phi_0^p) \tag{2.35}$$

$$\nabla S_{1w} = -\nabla S_{2w} \tag{2.36}$$

Using the Young formula to eleminate the surface tensions between the phases and the walls

$$\nabla \sigma_w = (\sigma_{1w} - \sigma_{2w}) = \sigma_{12} cos\alpha \tag{2.37}$$

Together with the equation for change in internal pressure when the volume of the phase is varied, this will result in an equation for energy. When this equation is minimised, the curvature of the interface is predicted.

The flow behaviour of two-phase laminar flow in a microchannel thus ranges from droplet-based flow to stratified flow with stable interface. The behaviour of the flow for two imiscible fluids can also be described by the dimensionless capillary number, Ca.

$$Ca = \frac{< u > \mu}{\sigma} \tag{2.38}$$

The capillary number gives the ratio between viscous forces and capillary forces. Capillary forces are forces that arise at the curved interface between two phases due to energy minimisation.

2.2. Mass transfer

To evaluate the extraction of perrhenate from the aqueous phase into the organic phase through the interface between the two phases, mass transfer theory needs to be understood.
Mass transfer is the net migration of mass over space and can be described at different scales. Diffusion is the intermingling of the atoms or molecules of more than one species; it is the inevitable result of the random, Brownian motions of the individual molecules that are distributed throughout space. Convection is migration of mass due to the bulk movement of the substance, and is the description of mass transfer at macro scale. Because laminar flow is characterised by high momentum diffusion and low momentum convection, diffusion will be elaborated on. [16]

2.2.1. Diffusive mass transfer

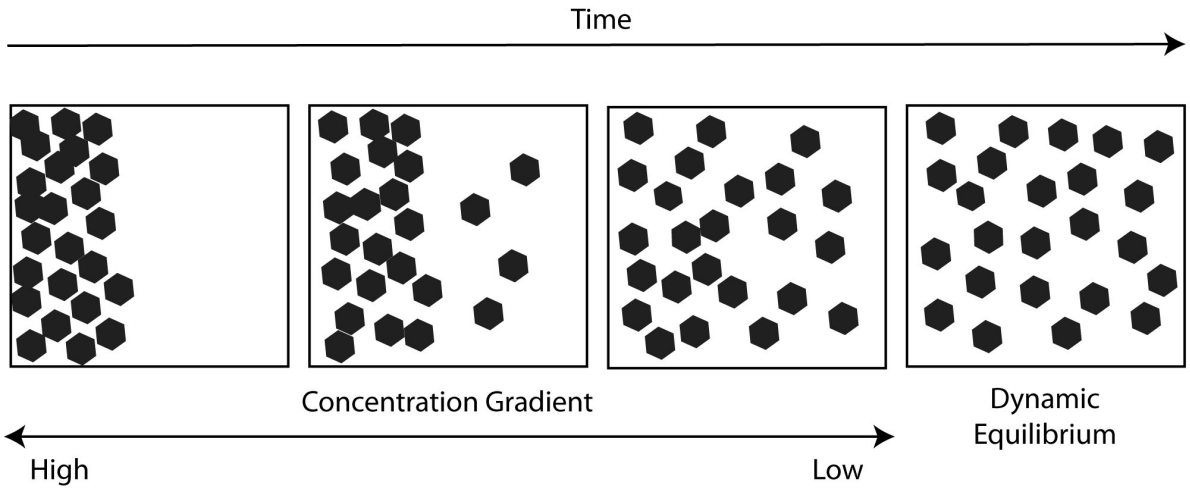

Figure 2.2: Schematic representation of particle diffusion. The black dots are molecules that diffuse from regions of high concentration to low concentration over time. [2]

Mass transfer in a solution can be described via different laws, but when a solution is dilute enough, Fick's laws can be used. The first law resides on the principle that the diffusive molar flux is proportional to concentration gradient, caused by a difference in chemical potential. Molecules move from a region with high

chemical potential, to a region of low chemical potential. Fick's first law describes the steady-state diffusive transport of molecules.

$$\phi_m = -D\frac{dc}{dx} \tag{2.39}$$

With ϕ_m the diffusive mass flux, D the diffusion coefficient and c the concentration.

Here, the diffusion coefficient is a number that is can be a strong function of composition. D can, in the dilute solution system, be regarded as a constant, and estimated from the kinetic theory of gases. This estimation is accurate when a binary, dilute system of nonpolar molecules is considered.
Fick's second law describes the change of concentation over time, caused by diffusion. The rate of change of concentration at a point in space is proportional to the second derivative of concentration with space, is Fick's law in words. Mathematically,

$$\frac{\partial c}{\partial t} = D\frac{\partial^2 c}{\partial x^2} \tag{2.40}$$

Fick's second law is derived by taking a mass balance over an infinitesmall layer from x to $x + dx$.

Estimation of diffusion coefficients Just as the description of the mass transfer can be done in different ways, so can the estimation of diffusion coefficients be done in multiple ways [**?**]. When in the binary system, the mole fraction of either of the components approaches unity, the solution can be thought of as infinitely dilute. Then, the diffusion coefficient can be estimated by the Stokes-Einstein equation

$$D_{12} = \frac{k_B T}{6\pi\mu_2 r_1} \tag{2.41}$$

Here, D_{12} is the diffusion coefficient of species 1 (the solute) infinitely diluted in species 2 (the solvent). k_B is Boltzmann's constant, T is the absolute temperature, μ is the dynamic viscosity of the solvent and r_1 is the radius of the diffusing molecule.

2.2.2. Mass transfer across an interface

For the perrhenate extraction, the assumption is made that the mass transfer is "slow", meaning that the character of the interface is not affected by the molecules that travel through it. The interface is located between the two different fluidic phases. When a solute is extracted, thus transferred, from an aqueous phase to an organic phase,

$$S_{aq} \leftrightarrows S_{org} \tag{2.42}$$

then the partitioning of the solute between the two phases is defined by the partition coefficient SOURCE [7]

$$K_D = \frac{[S_{org}]}{[S_{aq}]} \tag{2.43}$$

Where $[S_{org}]$ and $[S_{aq}]$ are the concentrations of the solute when equilibrium has been reached in the organic and aqueous phase, respectively.
The partitioning coefficient depends solely on the solubility and indicates the size of the difference in solubility of the solute in the two phases. A larger partitioning coefficient implies that the equilibrium lies more towards a higher concentration of the solute in the organic phase.
When there are multiple forms present of the solute, the distribution ratio is used to describe the ratios of the concentrations at chemical equilibrium. It considers the total concentration of the solute, including the concentrations of each different chemical form of the solute.

$$M = \frac{[S_{org}]}{\sum_{i=1}^{\infty} [S_{aq}]_i} \tag{2.44}$$

When the assumption is made that the interface offers zero resistance to mass transfer, equilibrium prevails at the interface.

$$[S_{org}] = M \sum_{i=1}^{\infty} [S_{aq}]_i \tag{2.45}$$

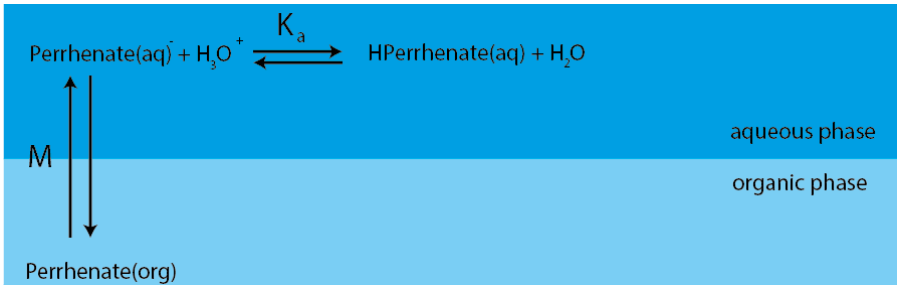

Figure 2.3: Schematic representation of the mass transfer and pH dependence of perrhenate by liquid-liquid extraction.

Because the concentration at the interface is now different when compared to the bulk concentration, there will be a chemical gradient thus a diffusive mass flux from the bulk phase towards the interface in the aqueous solution and a diffusive mass flux from the interface to the bulk in the organic phase.

pH dependency distribution ratio for ammonium perrhenate When the solute is part of an equilibrium reaction in one of the two phases, the distribution ratio and the partition coefficient do not coincide. In the distribution ratio, the role of the pH becomes apparent, when the equilibrium reaction is an acid-base reaction. In the following section, the pH dependency of the distribution ratio for ReO_4^- in aqueous solutions containing HCl is derived. In figure 2.3, a schematic representation is shown. The partition coefficient for ReO_4^-, is given as

$$K_D = \frac{\left[ReO_4^-\right]_{org}}{\left[ReO_4^-\right]_{aq}} \tag{2.46}$$

Here, the perrhenate comes from the solving of the NH_4ReO_4, which is a white crystalline salt:

$$NH_4ReO_4(s) \leftrightarrows NH_4(aq)^+ + ReO_4^-(aq) \tag{2.47}$$

In the aqueous phase, the following acid-base equilibrium reaction takes place

$$ReO_4^-(aq) + H_3O^+(aq) \leftrightarrows HReO_4(aq) + H_2O(l) \tag{2.48}$$

Where the H_3O is provided by the acid reaction, in which all the hydrogen of the hydrogenchloride reacts with water as hydrogrenchloride is a strong acid

$$HCl + H_2O \rightarrow H_3O^+ + Cl^- \tag{2.49}$$

In the acid-base equilibrium reaction 2.48, the location of the equilibrium depends on the pH. From the acid-base equilibrium reaction, the distribution ratio can be found

$$M = \frac{\left[ReO_4^-\right]_{org}}{[HReO_4]_{aq} + \left[ReO_4^-\right]_{aq}} \tag{2.50}$$

With the acid dissociation constant for $HReO_4$ given as

$$K_a = \frac{\left[H_3O^+\right]_{aq}\left[ReO_4^-\right]_{aq}}{[HReO_4]_{aq}} \tag{2.51}$$

This can be rewritten, yielding the distribution ratio in terms of the pH

$$M = \frac{\left[ReO_4^-\right]_{org}}{\left[ReO_4^-\right]_{aq}\left(1 + \frac{10^{-pH}}{K_a}\right)} \tag{2.52}$$

Thus, from formula 2.52 when the pH increases, the distribution ratio decreases.

3
Method

3.1. Microfluidic chip and extraction

In the experiment of Dalmázio and Oehlke, a microfluidic device was used with a Y inlet, main microchannel 12 [cm] of length and a Y splitter, as can be seen in the photographs in figure 3.1. The cross-section of the microchannel can be seen in as well in figure 3.1. The cross-section is not completely rectangular, but has circular indents at the bottom and a guide to help the laminar flow and stable interface develop.

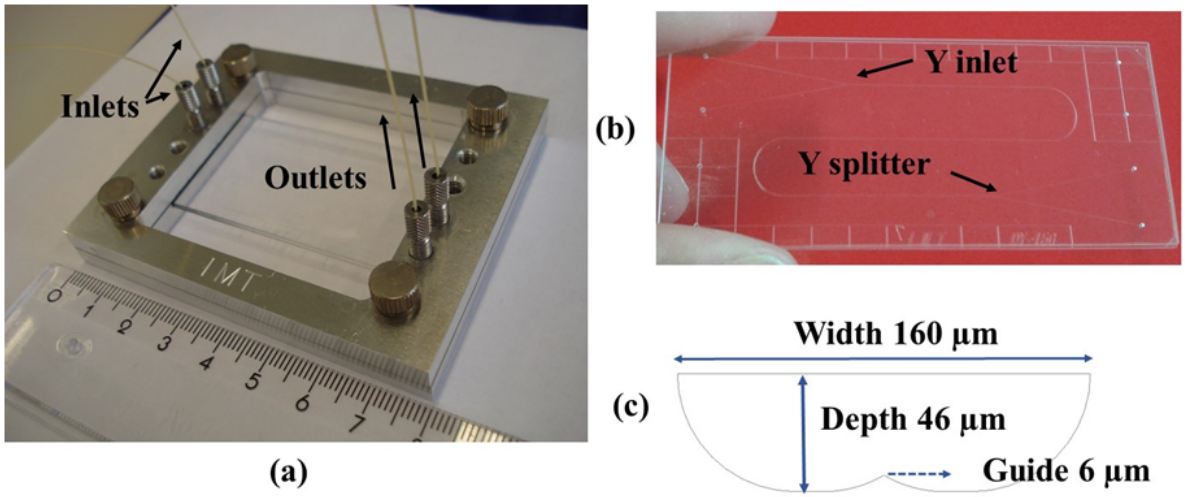

Figure 3.1: The chip that was used in the paper of Dalmázio and Oehlke. [5] (a) The entire microchip, with the syringes as in- and outlets. (b) The microchannel zoomed in on, with the main channel, Y inlet and Y outlet. (c) The cross section of the main channel.

The used feed solution was solved NH_4ReO_4 at 0.1 mg/mL in aqueous HCl solutions of different concentrations. The HCl concentrations were 0.01 [mol/L], 0.1 [mol/L] and 1 [mol/L]. Methyl-ethyl-ketone (MEK), also known as butanone was used as extractant. Furthermore, different flow rates and thus different contact times were used. These can be found in table 4.2 in the Results section. [5]

3.2. COMSOL

3.2.1. Mesh verification

COMSOL uses the finite element method (FEM) to compute approximate solutions for physical space- and time-dependent problems. These solutions are approximate because the partial differential equations (PDE) which describe the problem often cannot be solved analytically. An approximation to these equations based on numerical methods can be used. The model is partitioned into control surfaces to which the numerical

methods are applied. The total discretisation is also called the mesh, and one discretised surface a mesh element. When the model consists of more mesh elements, the computation time will grow. So, an appropriate meshing needs to be realised, while keeping the number of mesh elements as low as possible. This is done by checking whether or not the model is mesh dependent or not. The mesh is shown in figure 3.2

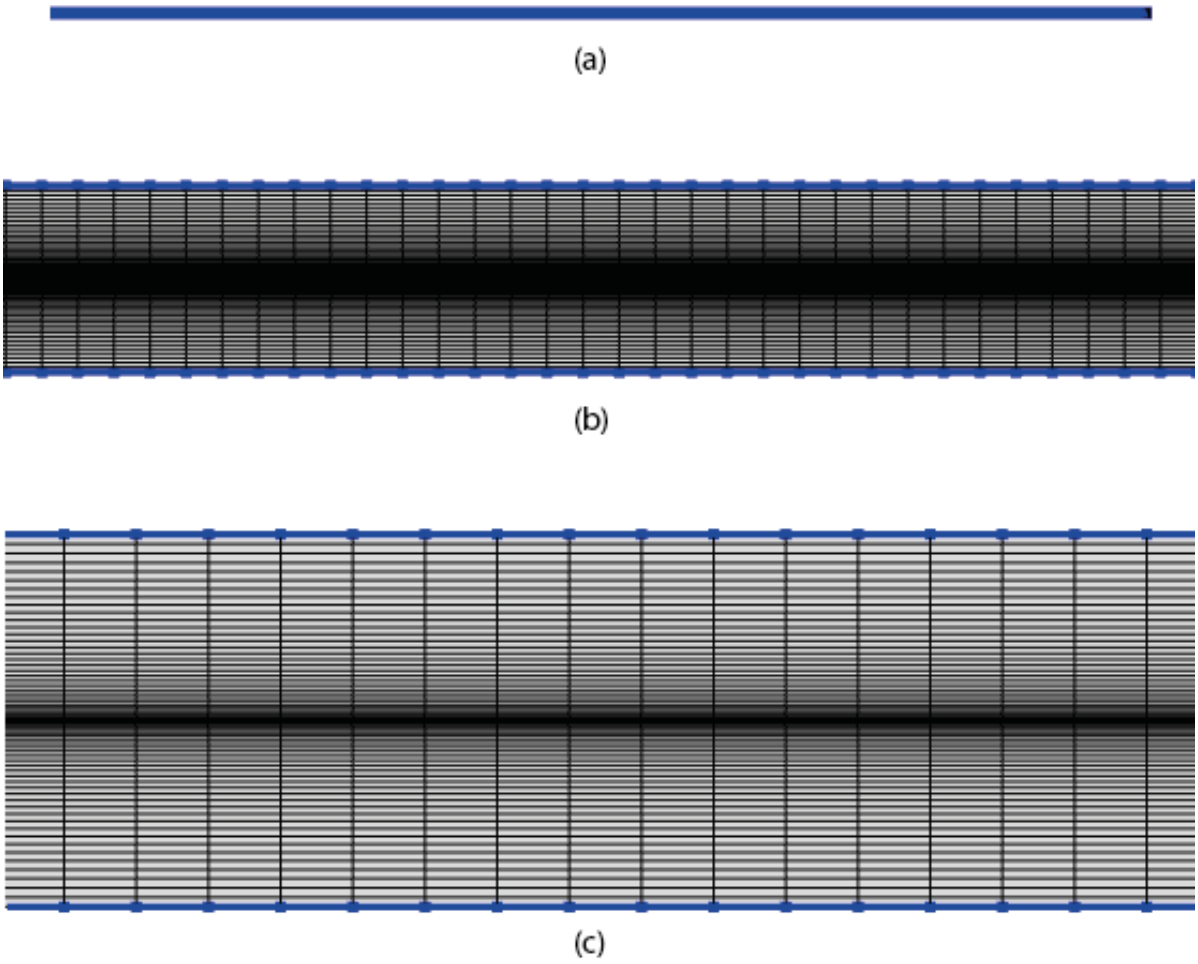

Figure 3.2: The meshed channel at different scales. (a) One tenth of the entire channel length is showed. The mesh elements are so small that they can't be distinguished. (b) Zoomed in further on the channel. As can be seen, in the x-direction, the mesh elements have the sime size over the entire channel. (c) Zoomed in further. Near the interface, the mesh elements become smaller in the y-direction, because the concentration gradient is greatest at the interface.

In vertical direction, the mesh will be denser towards the interface. This is because the gradient of the concentration is the greatest there so the PDE's need to be calculated over smaller distances. In horizontal direction, it has been found that the model is no longer mesh dependent when the number of mesh elements equals $L_{channel}/31$. By setting this in the model, when the length of the channel increases, the number of mesh elements increases proportionally with it, fixing the length of a mesh element in the horizontal direction, irregarding the length of the channel.

3.2.2. Modelling the extraction

To model the two-phase flow, the material properties have been defined space-dependently in a one-phase flow using one Laminar Flow module. This immediately fixes the interface spatially, at $y = 0$. The density and viscosity have been defined as follows in COMSOL

$$\rho = (y <= 0)(\rho_{org}) + (y => 0)(\rho_{aq}) \tag{3.1}$$

$$\mu = (y <= 0)(\mu_{org}) + (y => 0)(\mu_{aq}) \tag{3.2}$$

To model the extraction, several COMSOL multiphysics modules have been used. The Laminar Flow model was applied to account for the physics concerning the flow in the microchannel. In this module, at the inlet the laminar flow boundary condition was used and at the outlet the zero pressure boundary condition.

Next, to account for everything concerning the concentration, reaction and diffusion of the particles, two Transport of Diluted Species modules have been applied, one for each phase. Between the two modules, a Flux boundary condition has been set. This boundary condition defines that all the mass that leaves the aqueous phase, flows into the organic phase. In the upper Transport of Diluted Species module the boundary condition is defined as

$$Flux = k_d(M \cdot c_{aq} - c_{org}) \tag{3.3}$$

and in the lower Transport of Diluted Species module as

$$Flux = -k_d(M \cdot c_{aq} - c_{org}) \tag{3.4}$$

3.2.3. Calculating the extraction

When the solution has converged, the extraction efficiency is calculated by inserting the following formula in the Global Evaluation Parameter tab

$$\text{Extraction efficiency (EE)} = \frac{c_{org}^{out} \cdot u_{org}}{c_{aq}^{in} \cdot u_{aq}} \tag{3.5}$$

Where c_{org}^{out} is the concentration of perrhenate at the outlet in the organic phase, dependent on the y-coordinate, c_{aq}^{in} is the concentration of perrhenate in the aqueous phase at the inlet, dependent on the y-coordinate. c_{aq}^{in} is used because at the inlets, perrhenate is only present in the aqueous phase. u_{org} and u_{aq} are the flow rates in the organic and aqueous phase.

3.2.4. Leakage

Leakage from the organic phase to the aqueous phase was observed. The extraction efficiencies will be calculated both with and without taking the leakage into account. Taking the leakage into account is done as follows. In the processing of the data, this is accounted for by taking a cut line not over the full length of the outlet of the organic phase. In the other case, this leakage is not neglected because in the organic phase, the maximum concentration of the perrhenate is at the interface. This leakage is accounted for by taking a Cut Line not over the full length of the organic phase. It was estimated that the leakage is 25% of the organic phase and thus, from the photograph in figure 3.3.

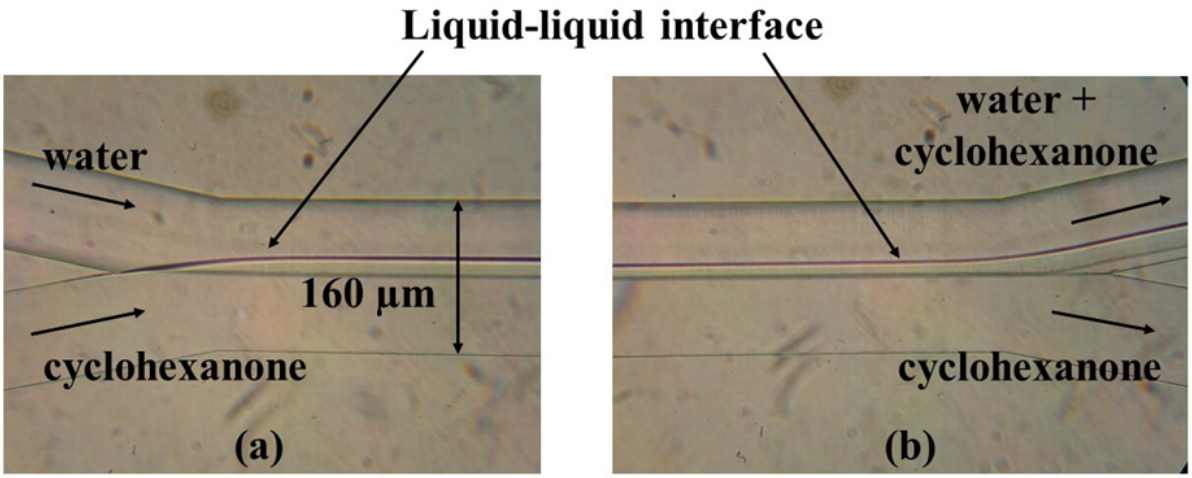

Figure 3.3: The observed leakage from the organic phase into the aqeuous phase from which the percentage leakage was estimated [5].

Hence, the Cut Line for the calculation of the perrhenate extraction efficiency via equation 3.5 was taken from $-h_{channel}/2$ to $-h_{channel}/8$. In figure 3.4, the cut line can be seen at the outlets.

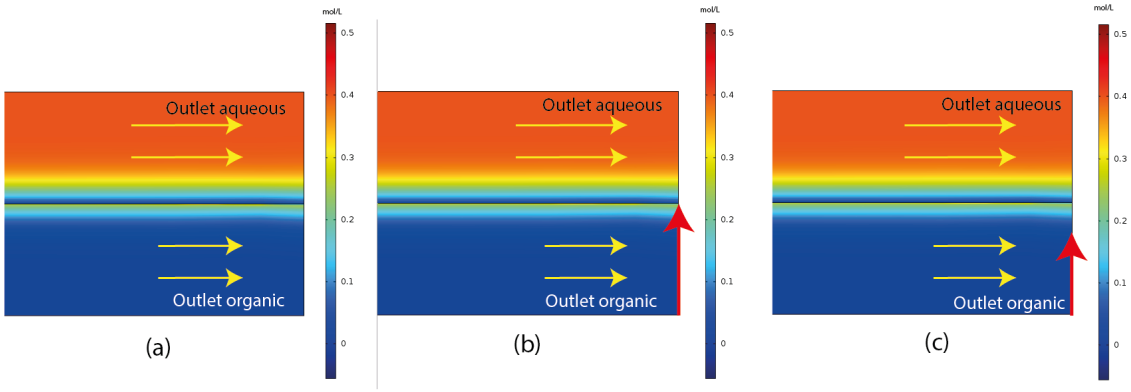

Figure 3.4: A representation how the leakage of the organic phase to the aqueous phase was taken into account at the end of the main channel. (a) The end of the main channel, with the yellow arrows depicting the velocity and the colours the concentration. Red is higher concentration and blue low. (b) The end of the main channel. The red arrow is the cut line for the situation without leakage taken into account. The cut line is taken over the entire y-length of the organic phase outlet. (c) The end of the main channel. The red arrow is the cut line for the situation with leakage taken into account. The cut line is taken over 3/4 of the y-length of the organic phase outlet.

3.2.5. COMSOL simplifications

To ensure that the simulation in COMSOL is possible, a few simplifications and assumptions have to be made.

2D vs 3D In the research done by P. Möller [11], it was found that the computed extraction efficiency does not differ significantly from 2D to 3D calculations. The small difference can be explained by the fact that the concentration of the solute is used in the calculation for the extraction efficiency and not the absolute ammount of perrhenate. Computing in 2D versus 3D saves a lot of computation time. [11]

Y inlet, main channel and Y splitter The glass chip, consisting of a Y inlet, main channel and Y splitter, is not fully considered in the simulation of the extraction. This is because the extraction solely takes place in the main channel. The two-phase flow is considered to be fully developed through the channel. This assumption is just because the distance for the flow to fully develop is insignificant, as will be shown in the Results section. Furthermore, in reality, this flow development too takes place.

Stable interface and leakage Dalmázio and Oehlke found that not for all flow rates, concentrations and compositions of the feed solution, a stable interface developed. In some situations, salting out effects could be observed. However, for the HCl feed solutions, a stable interface was observed. Hence, in the model, a stable interface is used, even though the aqueous solution and MEK are theoretically miscible.

3.3. Coefficients

Diffusion coefficients The diffusion coefficients are calculated by the Stokes-Einstein equation 2.41.

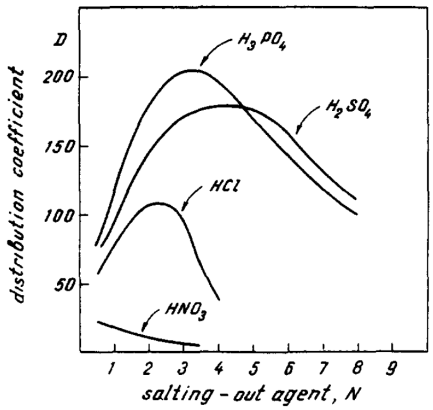

Figure 3.5: Experimental results based from the paper of Jordanov and Pavlova from which the distribution ratios will be estimated. [9]

3.3.1. Distribution ratios

To exactly calculate the needed distribution ratios, the reaction constants of the equilibrium reaction in the aqueous phase need to be known. However, these are not. Thus, the distribution ratios need to be predicted or based on experimental results. In the paper of Jordanov and Pavlova [9], the distribution ratios for different alkaline and acid media have been determined experimentally. The distribution ratios of perrhenate were measured radiometrically and photometrically. From the graphs 3.5, the distribution ratios for the different HCl concentrations were estimated. The estimated distribution ratios corresponding to the different HCl concentrations can be found in table A.1 in the Appendix. [9]

3.3.2. Mass transfer coefficients

The mass transfer coefficient $k_m$will be swept for two values, to check whether or not the model is dependent on it.

4

Results

The results section consists of multiple parts. The geometric assumptions will be evaluated. Next, the parametric sweep will be discussed quantitavely. Finally, the modelled results will be compared to the experimental results of Dalmázio and Oehlke [5].

Geometric assumptions In the COMSOL model, the channel has been designed as a microchannel with rectangular cross-section, with the dimensions in the Appendix A.2. In this way, the volumetric flow rates from the experiment of Dalmázio and Oehlke could easily be implemented. In reality, the channel has two semi-circular indents with a guide in between, as seen in Figure 3.1 in the section of Method. The total cross sectional area has been calculated by dividing the cross-section in several parts. In table 4.1 below, the cross-sectional area of the physical channel and the modelled channel is shown. [5]

Table 4.1: The cross-sectional areas for the modelled channel and the channel used in the experiment by Dalmázio and Oehlke [5]. The calculated percentage difference is 14.3%

What	Cross-sectional area
Modelled channel	7360 $(\mu m)^2$
Experimental channel	6306 $(\mu m)^2$

4.1. Parametric sweep

The parameters that will be swept are

1. the volumetric flow rate of both the aqueous and organic phases ($\dot{V}$)
2. the diffusion coefficient of ReO_4^- in the aqueous phase (D_{aq})
3. the diffusion coefficient of ReO_4^- in the organic phase (D_{org})
4. the distribution ratio (M)
5. the mass transfer coefficient (k_m)

The dimensions of the microfluidic channel will not be evaluated because the dimensions of the real life chip are known. Table 4.2 shows all the parameters that will be swept in the model. Each parameter will be combined with every other parameter so every possible combination is computed. The parameters that will be kept constant throughout the sweep can be found in table A.2 in the Appendix.

Table 4.2: The parameters over which the parametric sweep will run.

Parameter	**Unit**	**Values**				
M	[-]	1	10	35.29	35.33	44.12
		73.53	100	105.88	1000	
D_{aq}	m^2/s	$4.63 \cdot 10^{-13}$	$6.10 \cdot 10^{-13}$	$8.24 \cdot 10^{-13}$	$9.44 \cdot 10^{-13}$	$1.07 \cdot 10^{-12}$
D_{org}	m^2/s	$6.55 \cdot 10^{-13}$	$9.75 \cdot 10^{-13}$	$1.61 \cdot 10^{-12}$	$2.10 \cdot 10^{-12}$	$2.77 \cdot 10^{-12}$
$\dot{V}$	$\mu L/min$	20	30	40	50	
k_m	m/s	1	10			

The values of the flow rate are identical to the used flow rates in the experimental set-up. The distribution ratios are obtained from the paper of Jordanov and Pavlova, Figure 3.5.
The diffusion coefficients are obtained from equation 2.41 via the Stokes-Einstein relation, for different temperatures. In the table 4.3, the viscosities of both the aqueous and organic phase are given. For different temperatures, the viscosities are different and thus also the diffusion coefficients. The used atomic radius is $r_1 = 2.60 \cdot 10^{-10}[m]$ and the Boltzmann constant is given as $k_B = 1.38 \cdot 10^{-23}[m^2 kg s^{-2} K^{-1}]$

Table 4.3: The estimated diffusion coefficients using the Stokes-Einstein relation, to investigate the influence of the diffusion coefficient on EE. Varying the diffusion coefficient can, in reality, only be done by altering the temperature.

Absolute temperature	**Viscosity aqueous solution**	**Diffusion coefficient water**	**Viscosity MEK**	**Diffusion coefficient MEK**
K	$kg/(m \cdot s)$	m^2/s	$kg/(m \cdot s)$	m^2/s
275.15	1.67	$4.63 \cdot 10^{-13}$	1.18	$6.55 \cdot 10^{-13}$
283.15	1.31	$6.10 \cdot 10^{-13}$	0.82	$9.75 \cdot 10^{-13}$
293.15	1.00	$8.24 \cdot 10^{-13}$	0.51	$1.61 \cdot 10^{-12}$
298.15	0.89	$9.44 \cdot 10^{-13}$	0.40	$2.10 \cdot 10^{-12}$
303.15	0.80	$1.07 \cdot 10^{-12}$	0.31	$2.77 \cdot 10^{-12}$

These diffusion coefficients differ significantly from several experimental determined diffusion coefficients of copperchloride in aqueous solutions, which reside in the order of magnitude $1 \cdot 10^{-9}[m^2/s]$. Even though these experimentally derived values are for copperchloride in aqueous solutions and not organic compound, $D = 1 \cdot 10^{-9}[m^2/s]$ has been added as well in the parametric sweep for the comparison with the experimental results. For the qualitative evaluation of the parametric sweep, only the estimated diffusion coefficients via Stokes-Einstein are regarded. This is because the increase from $D = 1 \cdot 10^{-12}[m^2/s]$ to $D = 1 \cdot 10^{-9}[m^2/s]$ is not physically possible while keeping the same materials.

Viscosity The viscosities of both the aqueous and organic phases are not swept, because in the physics of mass transfer, they only appear in the determination of the diffusion coefficient by equation 2.41. They do play a role in the flow profile as determined in equation 2.25 and equation 2.26, but the distance for the flow profile to fully develop is negligible compared to the entire extraction length. In figure 4.1 below, the flow profile development in 1/250 of the channel is shown, in which it becomes clear that the flow develops really quickly.

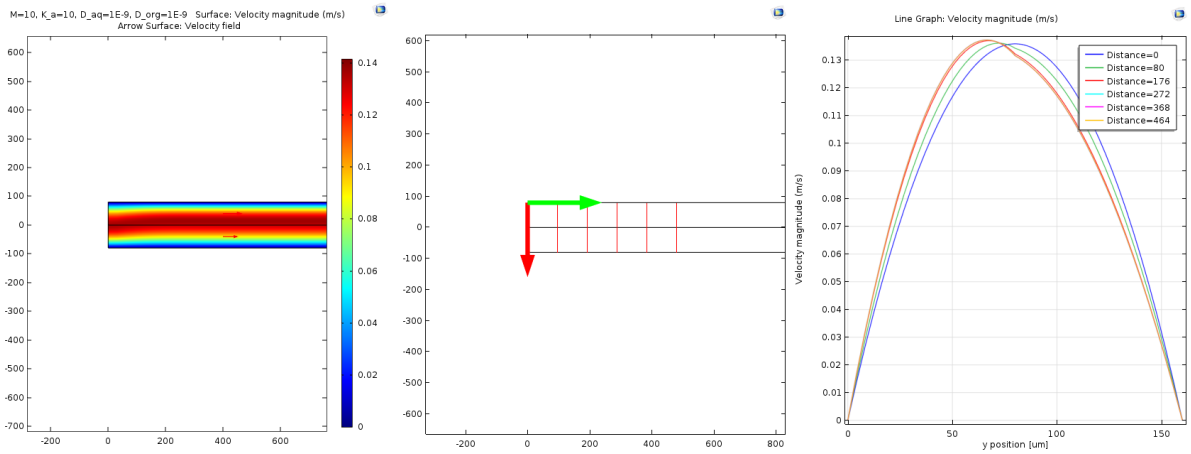

Figure 4.1: Several figures to show the flow rate development. (a) A 2D surface plot of the velocity through the channel. (b) To check the development, Cut Lines are added from the beginning of the main channel to 1/250 of the length of the channel. (c) The velocity profiles from the Cut Lines. As can be seen, the last three velocity profiles are identical, thus the flow has fully developed within 1/250 of the length of the main channel.

Flow rate dependency The modelled extraction efficiencies for the flow rates are shown in table 4.4. From the results, it becomes very clear that lower flow rates result in higher extraction efficiencies, irregarding the other parameters. This can logically be explained by the fact that lower flow rates mean longer contact times and thus more time for the diffusion through the interface.

Table 4.4: Some selected values to show the influence of the volumetric flow rate on the extraction efficiency. EE^A: extraction efficiencies with $D_{aq} = 1.07 \cdot 10^{-12} m^2/s$ and $D_{org} = 2.77 \cdot 10^{-12} m^2/s$. EE^B: extraction efficiencies with $D_{aq} = 1 \cdot 10^{-9} m^2/s$ and $D_{org} = 1 \cdot 10^{-9} m^2/s$. $\Delta_{abs}\dot{V}$ is the absolute change in flow rate in $\mu L/min$, $\Delta_{rel}\dot{V}$ is the relative change in flow rate in %. EE_{abs} is the absolute change in extraction efficiency and EE_{rel} is the relative change in extraction efficiency when the flow rate is altered.

$\dot{V}$ $\mu L/min$	EE^A	EE^B	$\Delta_{abs}\dot{V}$	$\Delta_{rel}\dot{V}$	EE_{abs}	EE_{rel}
20	0.081	57.298				
30	0.045	49.198	10	50.00	-0.035	-43.929
40	0.038	44.123	10	33.33	-0.008	-16.685
50	0.035	40.587	10	25.00	-0.003	-6.891

Distribution ratio dependency From the modelled result, it can be seen that the equilibrium at the interface is indeed set by the distribution ratio. In figure 4.2 it can be seen that at the interface, the concentration of c_{org} is M times c_{aq}, for each M.

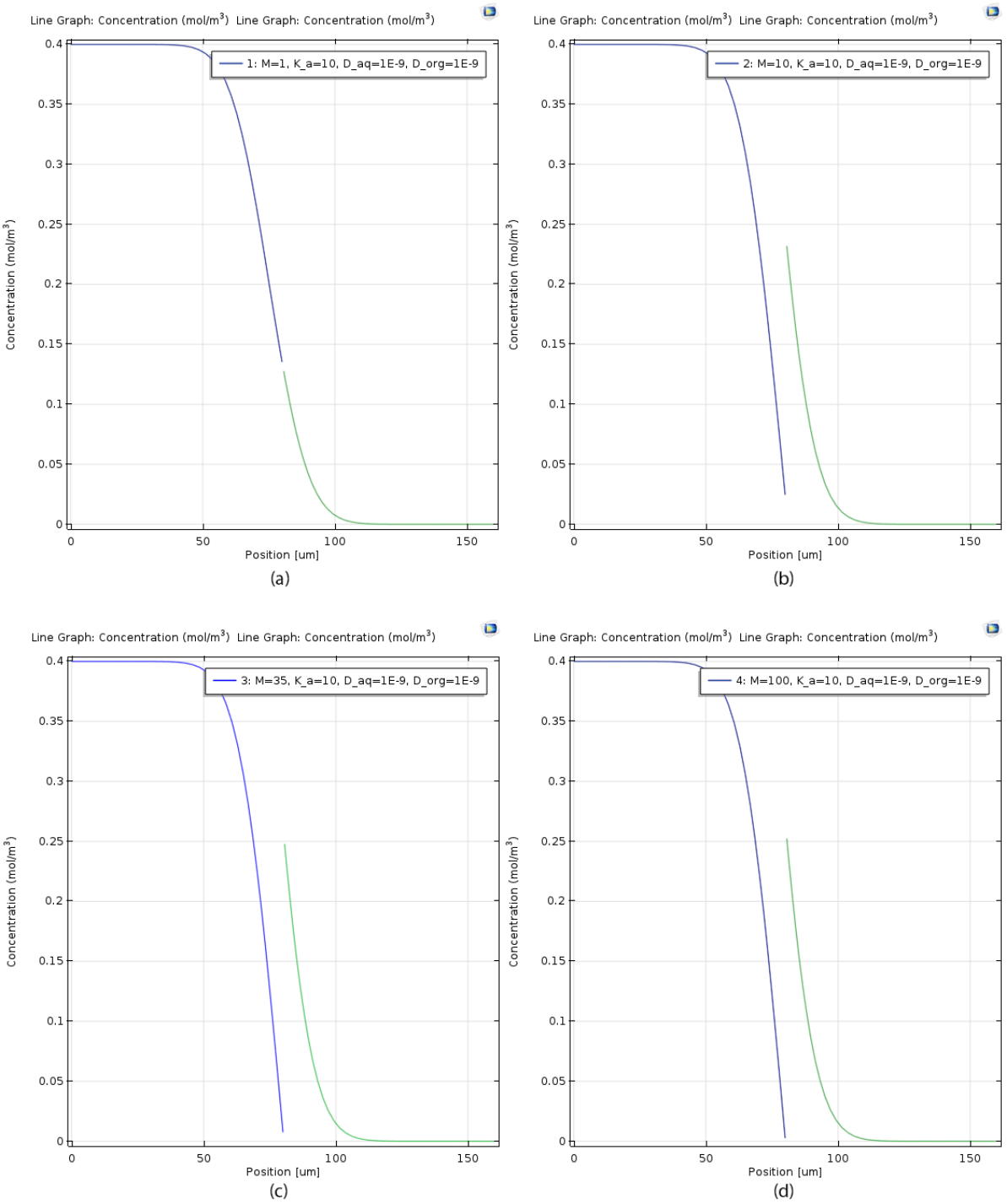

Figure 4.2: The concentration profiles through the channel for different distribution ratios. The other parameters are held constant at $K_m = 1m/s$, $\dot{V} = 20\mu L/min$ $D_{aq} = 1 \cdot 10^{-9} m^2/s$ and $D_{org} = 1 \cdot 10^{-9} m^2/s$. The cut lines are taken 60000 μm from the inlet. (a) $M = 1$. (b) $M = 10$. (c) $M = 35$. (d) $M = 100$.

From the results of the parametric sweep, a relationship between the distribution ratio and the extraction efficiency can be deduced, as shown in figure 4.3 below.

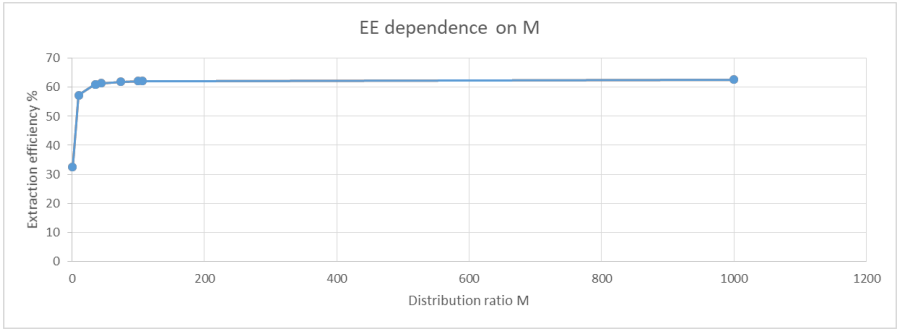

Figure 4.3: The dependence of the extraction efficiency on the distribution ratio M without the leakage accounted for. In the range $M = 1-40$, the extraction efficiency is sensitive to M. The used flow rate was $20\mu L/min$ and the used diffusion coefficients $D_{aq} = D_{org} = 1 \cdot 10^{-9} m^2/s$

Diffusion coefficient dependency In the Appendix, table 4.5 and table 4.6, the extraction efficiencies are given while the diffusion coefficient was swept for the estimated values. It is shown that increasing D_{aq} makes more of a difference than increasing D_{org}. This can be explained by the fact that the flux is driven by the concentration difference, with the concentration of perrhenate in the aqueous phase multiplied by the distribution ratio. Thus, the concentration of perrhenate in the aqueous phase has a bigger impact on the mass flux through the interface and in this way also on the extraction efficiency.

Table 4.5: Some selected values to show the influence of D_{aq} on the extraction efficiency for $M = 10$ and $\dot{V} = 20\mu L/min$. $\Delta_{abs}D_{aq}$ is the absolute change in diffusion coefficient of the aqueous phase in m^2/s and $\Delta_{rel}D_{aq}$ is the relative change in diffusion coefficient of the aqueous phase in %.

$\mathbf{D_{aq}}$ m^2/s	**EE** %	$\mathbf{\Delta_{abs}D_{aq}}$ m^2/s	$\mathbf{\Delta_{rel}D_{aq}}$ %	$\mathbf{EE_{abs}}$ %	$\mathbf{EE_{rel}}$
$4.63{\cdot}10^{-13}$	0.0526				
$8.24{\cdot}10^{-13}$	0.0641	$3.61{\cdot}10^{-13}$	78.0	0.0114	21.73
$9.44{\cdot}10^{-13}$	0.0756	$1.20{\cdot}10^{-13}$	14.6	0.0115	18.01
$1.07{\cdot}10^{-12}$	0.0806	$1.26{\cdot}10^{-13}$	13.3	0.0050	6.58

Table 4.6: Some selected values to show the influence of D_{org} on the extraction efficiency for $M = 10$ and $\dot{V} = 20\mu L/min$. $\Delta_{abs}D_{org}$ is the absolute change in diffusion coefficient of the organic phase in m^2/s and $\Delta_{rel}D_{org}$ is the relative change in diffusion coefficient of the organic phase in %.

$\mathbf{D_{org}}$ m^2/s	**EE** %	$\mathbf{\Delta_{abs}D_{org}}$ m^2/s	$\mathbf{\Delta_{abs}D_{org}}$ %	$\mathbf{EE_{abs}}$ %	$\mathbf{EE_{rel}}$
$6.55{\cdot}10^{-13}$	0.0790				
$9.75{\cdot}10^{-13}$	0.0795	$3.20{\cdot}10^{-13}$	48.9	0.00048	0.6077
$1.61{\cdot}10^{-12}$	0.0799	$6.35{\cdot}10^{-13}$	65.1	0.00042	0.5289
$2.09{\cdot}10^{-12}$	0.0802	$4.80{\cdot}10^{-13}$	29.8	0.00025	0.3185
$2.77{\cdot}10^{-12}$	0.0806	$6.80{\cdot}10^{-13}$	32.5	0.00041	0.5095

Leakage Some qualitative results can be drawn from the difference between the modelled extraction with and without the leakage. In table 4.7 below, the modelled extraction efficiencies with and without the leakage accounted for are shown.

Table 4.7: Comparison of modelled extraction efficiencies with and without leakage accounted for. Only modelled extraction efficiencies are shown just to show the influence of the leakage on the modelled extraction. $\dot{V} = 20\mu L/min$, $D_{aq} = D_{org} = 1 \cdot 10^{-9} m^2/s$

Distribution ratio	EE leakage	EE no leakage	Difference	% Difference
1	14.46	32.42	17.96	224.13
10	25.04	57.30	32.26	228.85
35.29	26.72	61.08	34.36	228.62
44.12	26.79	61.40	34.61	229.20
73.53	27.10	61.92	34.83	228.54
100	27.19	62.13	34.94	228.52
105.88	27.20	62.16	34.96	228.51

It can be seen that the percentage difference, irregarding the distribution ratio, is around 225%. Due to the 25% leakage from the organic phase to the aqueous phase, the extraction efficiency decreases 2.25 times on average.

4.2. Comparison

In table 4.8 in the appendix, the experimental extraction efficiencies are shown together with the modelled extraction efficiencies and the difference, swept for different flow rates. The distribution ratios that were used for the modelling were estimated from figure 3.5 in the Method section, by fitting the values linearly on the part of the graph that grows linearly.

Table 4.8: Comparing the experimental results to the modelled results for multiple flow rates and HCl concentrations without leakage accounted for. $D_{aq} = D_{org} = 1 \cdot 10^{-9} m^2/s$. The estimated distribution ratios M corresponding to the different HCl concentrations that were used can be found in table A.1

$\dot{V}$	[HCl]	Experimental EE	Modelled EE	M	ΔEE_{abs}
$\mu L/min$	mol/L	%	%	-	%
20.00	0.00	3.00	61.08	35.29	58.08
20.00	0.01	25.00	61.08	35.33	36.08
20.00	0.10	32.00	61.40	44.12	29.40
20.00	1.00	52.00	61.92	73.53	9.92
30.00	0.00	1.00	52.47	35.29	51.47
30.00	0.01	18.00	52.47	35.33	34.47
30.00	0.10	21.00	52.74	44.12	31.74
30.00	1.00	43.00	53.19	73.53	10.19
40.00	0.00	1.00	47.06	35.29	46.06
40.00	0.01	14.00	47.06	35.33	33.06
40.00	0.10	15.00	47.30	44.12	32.30
40.00	1.00	39.00	47.71	73.53	8.71
50.00	0.00	2.00	43.28	35.29	41.28
50.00	0.01	12.00	43.28	35.33	31.28
50.00	0.10	14.00	43.51	44.12	29.51
50.00	1.00	36.00	43.88	73.53	7.88

It is obvious that the results definetely do not coincide. What becomes clear, is that the difference in extraction efficiency decreases with the HCl concentration. From table 4.8 it can also be concluded that the extraction efficiency of the experiment depends on the HCL concentration differently then the way the modelled extraction efficiency depends on the estimated distribution ratios.

To find an analogue beteen the dependency of the real-life extraction efficiency on the HCl concentration and the modelled extraction efficiency on the distribution ratio, the dependence of the extraction efficiency on the HCl concentration is shown in figure 4.4, for the four flow rates.

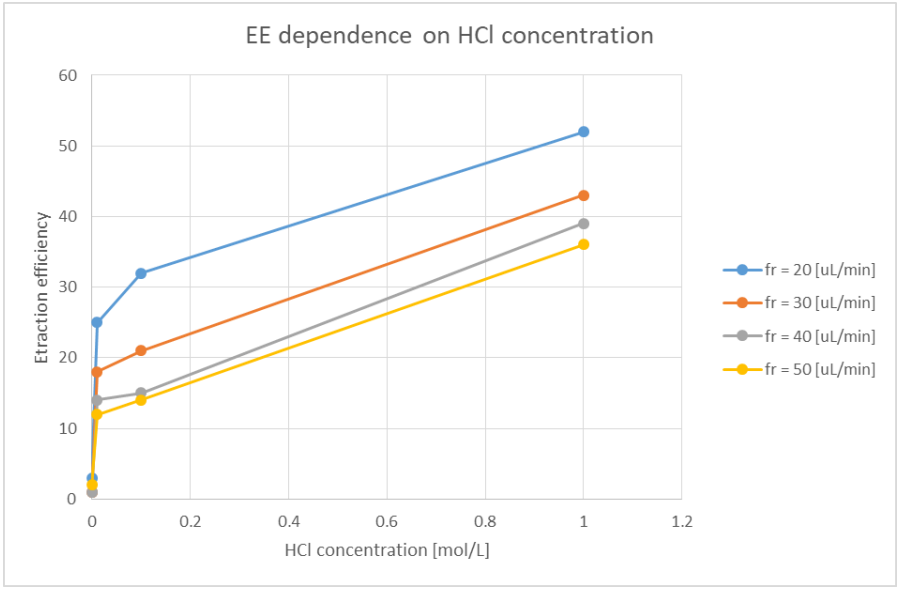

Figure 4.4: The dependence of the experimentally determined extraction efficiency on the HCl concentrations by Dalmázio and Oehlke.

The graphs for the experimental extraction efficiency and the modelled extraction efficiency have the same form, exponential, only the graph for the modelled extraction efficiency has an offset, so the modelled extraction efficiency starts higher. What is also striking, is that via the theory, it is expected that the extraction decreases with decreasing pH. From the experimental results, the reverse behaviour is observed.

Matching When the leakage is accounted for as described in the Method section, for the case with $D_{org} = D_{aq} = 1 \cdot 10^{-9}[m^2/s]$ and HCl concentration of $0.01[mol/L]$, the experimental result and the modelled result happen to fit quite nicely. The difference between the experimental extraction efficiency and the modelled extraction efficiency is just 1.7% as can be seen in figure 4.5. However, for the other estimated distribution ratios it does not coincide, probably due to the offset of distribution ratios in the above derived relationship between the extraction efficiency and the distribution ratio. The modelled results do depend on the distribution ratio, as can be seen in figure 4.3, but in this model this cannot be seen because the distribution ratios were apparently incorrectly estimated for the corresponding HCl concentrations. The estimated distribution ratios reside already in the range where the the extraction efficiency is no longer sensitive to the distribution ratio, which can be seen in the graph in figure 4.3.

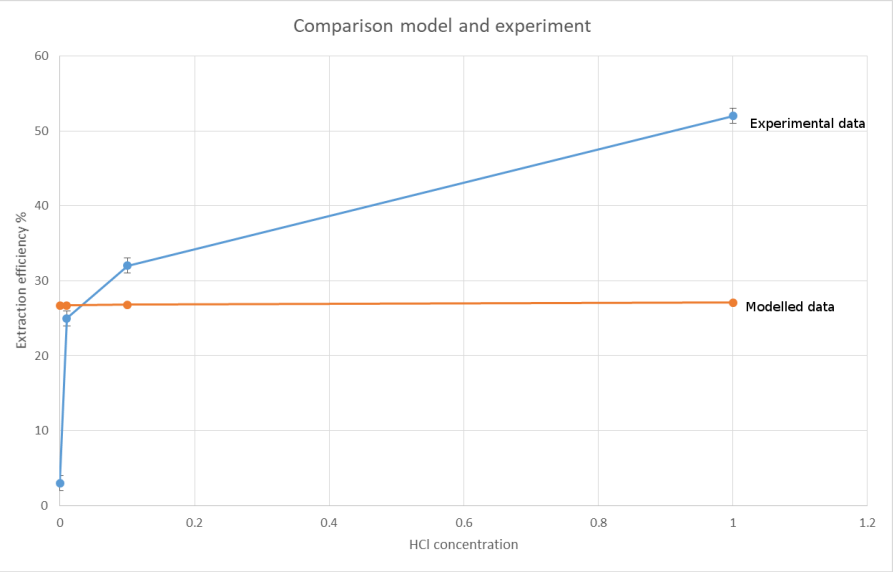

Figure 4.5: Comparing the modelled results to the experimental results of Dalmázio and Oehlke. $D_{aq} = D_{org} = 1 \cdot 10^{-10} m^2/s$ and $\dot{V} = 20 \mu L/min$ The results only coincide for one value. The blue line is the data from the experiment of Dalmázio and Oehlke, the orange line from the model with the leakage accounted for.

5

Conclusions

This section draws conclusions derived from the Results section. First, the general conslusions of the comparison will be stated. Also conclusions on the parametric sweep will be made. Lastly, some conclusions will be drawn about the leakage.

Conclusions about the distribution ratio From the theory, it is expected that the distribution ratio increases when the pH is increased. Then, from the parametric sweep, it was found that for higher distribution ratios, the extraction efficiency would be higher. However, when comparing this with the experimental results of Dalmázio and Oehlke, this is not the case, the inverse is observed. This can be assigned to the fact that possibly not perrhenate, but perrhenic acid can be extracted by MEK. Then in the organic phase, the perrhenic acid dissociates leaving the perrhenate ions in the organic phase.

When this is assumed, the partition coefficient and distribution ratio's will be considered for the perrhenic acid and will yield

$$K_D = \frac{[HReO_4]_{org}}{[HReO_4]_{aq}} \tag{5.1}$$

$$M = \frac{[HReO4]_{org}}{[HReO_4]_{aq}\left(1 + \frac{K_a}{10^{-pH}}\right)} \tag{5.2}$$

From this equation, it can be seen that when the pH increases, the distribution ratio and thus the extraction of the perrhenic acid increases, leaving more perrhenate in the organic phase. Thus increasing too the extraction efficiency of the perrhenate itself. This agrees with the results from the experiment and the parametric sweep.

The experimental result by Dalmázio and Oehlke [5] shows a behaviour of the extraction efficiency depending on the HCl concentration that looks similar to the behaviour of the modelled extraction efficiency depending on the distribution ratio, only with an offset. This indicatse that the estimation of the distribution ratio based on the paper is not done correctly for low salting out agents.

The dependency of the extraction efficiency on the distribution ratio is exponential asymptotic. When the distribution ratio increases from zero to a little number, the extraction efficiency also increases the fastest. This can be explained by the fact that, in the model, the flux is defined as in equation 3.3, where the concentration in the aqueous phase is multiplied with the distribution ratio. When the distribution ratio is already quite high, and is increased even further, the relative impact is not big. So, when the distribution ratio exceeds physical values, the extraction efficiency will not increase that much.

Mass transfer coefficient Sweeping for the mass transfer coefficient does not result in different extraction efficiencies. This can be explained by the fact that even though it results in an different flux size in absolute terms through the interface as in equation 3.3, the relative concentrations between the two phases only depend on the distribution ratio. The theory also predicts this; the percentage of the extracted perrhenate only depends on the difference in concentration due to Fick's law in equation 2.39. Thus, the mass transfer coefficient can in this model be regarded as a coefficient just to assign the right units to the flux in the model.

Conclusions about the diffusion coefficient The extraction efficiencies as calculated using the diffusion coefficients via the Stokes-Einstein relation diverged vastly from the real experimental results. This suggests that using the Stokes-Einstein relation in this situation is not a good method of estimating the diffusion coefficients. In retrospect, this can be assigned to the fact that Stokes-Einstein is valid when the radius of the solute is really big compared the radius of the solvent molecules. In this case, the radii are in the same order of magnitude for the aqueous phase and the radius of the solute is even smaller than the radius of the solute, resulting in big errors in the estimation. The Stokes-Einstein equation is only valid when the diffusing molecules are very large compared to the solvent molecules. [stokes] Furthermore, increasing the aqueous diffusion coefficient has the highest impact on the extraction efficiency.

Conclusions about the leakage When diffusion coefficients, based on experimental measurements, were assigned to the two phases, the extraction efficiencies appeared already more viable. For these outcomes, the extraction efficiencies are evaluated for the leakage of the organic phase to the aqueous phase. Even though it is less harmful for the organic phase to flow to the aqueous phase as then there is no pollution, the results show that the extraction efficiencies decrease drastically. Even when the leakage is, as in our model, a quarter of the cross-sectional length of the organic outlet, the extraction efficiency decreases by more than 100% This is quite logical, as the conenctration profiles in figure 4.2 reveal that the concentration of perrhenate in the organic phase is highest near the interface. Which is exactly the part of the liquid that is lost by leakage. The extraction efficiency can however be increased drastically by ensuring that the leakage from the organic phase to the aqueous phase does not occur.

6

Recommendations

This research has delivered results, but these were delivered under quite some assumptions, estimations and restrictions. Also, some estimation errors have been made. Due to this, the results do not agree with the physics happening in reality. The recommendations section will elaborate on possibilities to extend this research to overcome its shortcomings.

6.1. Improvements

Simulating the interface with a real two-phase flow In the experiment by Dalmázio and Oehlke, a stable interface was established but leakage was observed. For the modelling, the leakage was estimated by eye based on a picture of the microfluidic channel. This is of course not very accurate. To find a more quantitative influence of the leakage on the extraction rate, the amount of leakage needs to be determined more precisely. One way to achieve this, is to model with a real two-phase flow in COMSOL and only consider Fluid Dynamics modules to focus on this particular subject. Then probably, the influence of the flow rates and viscosities will also be greater because these parameters then also alter the interface thus the contact area of the extraction.

Estimating interface curvature and then implementing this in the geometry In this research, the calculations have been performed 2D. Previous done research has proven for a flat interface that the extraction efficiencies do not differ significantly between 2D and 3D. However, in reality the interface is not flat but curved because of the minimisation of energy in which the surface tension plays a big role on microscale. The computation time increases significantly when switching to 3D, so by taking a lot of time for the computations this can be done. Else, the increase in interface area by the curvature can maybe be accounted for in the 2D case as well. The interface curvature can be calculated, and the percentage increase compared to a flat interface as well. By tweaking parameters such as the diffusion coefficient, the extraction efficiency can be calculated.

Distribution ratios It was concluded that the estimation of the distribution ratios was not done correctly. To overcome this shortcoming, it is suggested to also sweep the model for $M = 0\sim1$.

Test the numerical results to other experimental results The model has been tested to the extraction of perrhenate using MEK because the distribution ratios could be estimated quite well for this compound. To test the model even more/gain more insight, it can also be tested to other compounds which were experimented with by Dalmázio and Oehlke. When the numerical results coincide with the experimental results, the distribution ratios could be estimated using the computational model.

6.2. Further research

Whether or not microfluidic solvent extraction is feasible for the production of radionuclides can be investigated further.

Other microfluidic devices Microfluidic devices with other geometric shapes can possibly increase the extraction efficiency. $\psi - \psi$-shaped microchannels, $Y - \psi$-shaped or even other shaped can be simulated. In the ψ shaped chips, there are three inlets and outlets, thus two interfaces and a shorter diffusion path when the middle inlet is used for the aqueous phase. In these chips, however, the interface control might be a big challenge.

Other solvents From the results it has been concluded that not the $ReO4^-$ was the molecule that diffuses through the liquid-liquid interface, but actually the $HReO_4$. Even though in this way, the perrhenate can also be extracted, it might be interesting to investigate other compounds for which the perrhenate diffuses through the interface and not the perrhenic acid.

A

Appendix A - constants

Table A.1: The estimated distribution ratios for the different HCl concentrations used in the experiment by Dalmázio and Oehlke [5]. The distribution ratios were estimated from figure 3.5 [9]

Concentration HCl mol/L	**pH**	**Estmated distribution ratio**
0	7	35.29
0.01	2	35.33
0.1	1	44.12
1	0	73.53

Table A.2: The properties of the microchannel, aqueous phase and organic phase that are kept constant throughout the parametric sweep.

Parameter	**Value**	**Unit**
Extraction channel dimensions		
L	12	cm
h	160	um
z	46	um
Aqueous phase		
ρ_{aq}	1000	kg/m^3
μ_{aq}	1.00	$mPa \cdot s$
$[ReO_4^-]$	$4.00 \cdot 10^{-4}$	mol/L
Organic phase		
ρ_{org}	804.9	kg/m^3
μ_{org}	0.51	$mPa \cdot s$
$[ReO_4^-]$	0	mol/L

B

Appendix B - results

Table B.1: A selection of the big data obtained from the parametric sweep.

$\dot{V}$	M	k_m	D_{aq}	D_{org}	EE
$\mu L/min$	-	m/s	m^2/s	m^2/s	-
20	105.88	10	$1.07 \cdot 10^{-13}$	$2.77 \cdot 10^{-12}$	0.212
20	105.88	10	$9.44 \cdot 10^{-13}$	$2.77 \cdot 10^{-12}$	0.208
50	105.88	10	$1.07 \cdot 10^{-12}$	$2.77 \cdot 10^{-12}$	0.201
20	73.529	10	$1.07 \cdot 10^{-12}$	$2.77 \cdot 10^{-12}$	0.199
40	105.88	10	$1.07 \cdot 10^{-12}$	$2.77 \cdot 10^{-12}$	0.198
30	105.88	10	$1.07 \cdot 10^{-12}$	$2.77 \cdot 10^{-12}$	0.198
40	105.88	10	$9.44 \cdot 10^{-13}$	$2.77 \cdot 10^{-12}$	0.197
50	105.88	10	$9.44 \cdot 10^{-13}$	$2.77 \cdot 10^{-12}$	0.197
30	105.88	10	$9.44 \cdot 10^{-13}$	$2.77 \cdot 10^{-12}$	0.196
20	73.52	10	$9.44 \cdot 10^{-13}$	$2.77 \cdot 10^{-12}$	0.195
50	73.52	10	$1.07 \cdot 10^{-12}$	$2.77 \cdot 10^{-12}$	0.184
30	73.52	10	$1.07 \cdot 10^{-12}$	$2.77 \cdot 10^{-12}$	0.182
40	73.52	10	$1.07 \cdot 10^{-12}$	$2.77 \cdot 10^{-12}$	0.182
40	73.52	10	$9.44 \cdot 10^{-13}$	$2.77 \cdot 10^{-12}$	0.181
30	73.52	10	$9.44 \cdot 10^{-13}$	$2.77 \cdot 10^{-12}$	0.181
50	73.52	10	$9.44 \cdot 10^{-13}$	$2.77 \cdot 10^{-12}$	0.180
20	35.29	10	$1.07 \cdot 10^{-12}$	$2.77 \cdot 10^{-12}$	0.160
20	35.29	10	$9.44 \cdot 10^{-13}$	$2.77 \cdot 10^{-12}$	0.155
30	35.29	10	$1.07 \cdot 10^{-12}$	$2.77 \cdot 10^{-12}$	0.139
30	35.29	10	$9.44 \cdot 10^{-13}$	$2.77 \cdot 10^{-12}$	0.137
50	35.29	10	$1.07 \cdot 10^{-12}$	$2.77 \cdot 10^{-12}$	0.136
40	35.29	10	$1.07 \cdot 10^{-12}$	$2.77 \cdot 10^{-12}$	0.136
40	35.29	10	$9.44 \cdot 10^{-13}$	$2.77 \cdot 10^{-12}$	0.135
50	35.29	10	$9.44 \cdot 10^{-13}$	$2.77 \cdot 10^{-12}$	0.132
20	1	10	$9.44 \cdot 10^{-13}$	$2.77 \cdot 10^{-12}$	0.031
20	1	10	$1.07 \cdot 10^{-12}$	$2.77 \cdot 10^{-12}$	0.030
30	1	10	$9.44 \cdot 10^{-13}$	$2.77 \cdot 10^{-12}$	0.015
30	1	10	$1.07 \cdot 10^{-12}$	$2.77 \cdot 10^{-12}$	0.014
50	1	10	$1.07 \cdot 10^{-12}$	$2.77 \cdot 10^{-12}$	0.008
40	1	10	$9.44 \cdot 10^{-13}$	$2.77 \cdot 10^{-12}$	0.007
40	1	10	$1.07 \cdot 10^{-12}$	$2.77 \cdot 10^{-12}$	0.006
50	1	10	$9.44 \cdot 10^{-13}$	$2.77 \cdot 10^{-12}$	0.006

Bibliography

[1] *Detailed guidance on the European clinical trials database (EUDRACT Database).*

[2] Hartnell college biology tutorials. Online tutorials.

[3] A. Blok. Extraction of technetium-99m. Bachelors thesis.

[4] H. Bruus. *Theoretical Microfluidics.* Oxford University Press, 2007.

[5] Ilza Dalmázio and Elisabeth Oehlke. Microfluidic extraction of radioactive perrhenate from acid solutions using cyclohexanone. *International Nuclear Atlantic Conference*, 2017.

[6] Bruce A. Finlayson. Poiseuille flow of two immiscible fluids between flat plates with applications to microfluidics. *University of Washington*, -.

[7] David Harvey. Liquid-liquid extractions. Technical report, DePauw University, 2017.

[8] L. Janssen and M. Warmoeskerken. *Transport Phenomena Data Companion.* Edward Arnold, 2006.

[9] N. Jordanov and M. Pavlova. Study of liquid-liquid extraction of perrhenate with cyclohexanone in different media. *Pergamon Press*, 1976.

[10] Maria Andreou Maria Argyrou, Alexia Valassi and Maria Lyra. Rhenium-188 production in hospitals, by w-188/re-188 generator, for easy use in radionuclide therapy. *International Journal of Molecular Imaging*, 2013.

[11] P. Möller. Investigating the selective separation ability of an optimized microfluidic chip with focus on metal ions. Bachelors thesis.

[12] J. Rovinsky N. Brauner and D. Moalem Maron. Determination of the interface curvature in stratified two-phase systems by energy considerations. *Elsevier Science*, 1996.

[13] Klaus Schwochau. *Technetium: Chemistry and Radiopharmaceutical Applications*, chapter 6 Some fundamentals of technetium chemistry, page 43. John Wiley & Sons, 2008.

[14] M.S.P. Stevar. Shapes and dynamics of miscible liquid/liquid interfaces in horizontal capillary tubes. Online published.

[15] D.J. Triton. *Physical Fluid Dynamics.* Oxford Science Publications, 1977.

[16] H. van den Akker and R. Mudde. *Transport Phenomena.* Delft Academic Press, 2014.